Optically Profiling a Draining Aqueous Film Confined between an Oil Droplet and a Solid Surface: Effect of Nonionic Surfactant

Chor Sing Tan,[†,‡] Michelle L. Gee,*[,†] and Geoffrey W. Stevens[‡]

School of Chemistry and Department of Chemical Engineering, University of Melbourne, Parkville 3010, Victoria, Australia

Received December 18, 2002. In Final Form: April 2, 2003

We have profiled the deformation of an oil droplet during its approach to a silica surface, monitoring the drainage of the intervening aqueous film in real time, using imaging ellipsometry/reflectometry. Specifically, we investigated how film drainage and droplet deformation are affected by the addition of the nonionic surfactant $C_{12}E_8$. The droplet dimples at the beginning of film drainage at its center. At low surfactant concentrations (<10% of the cmc) we observe film recovery, due to the Marangoni effect reversing the direction of fluid flow. High surfactant concentrations minimize interfacial tension gradients, thereby hindering Marangoni flow. Lowering of the oil−water interfacial tension promotes spreading at the barrier ring and nonuniform film drainage; i.e., the dimple "sweeps" across the film profile. The rate of drainage can be explained in terms of the Hagen−Poiseuille law and, as such, is dependent on the extent to which spreading occurs and the hydrostatic pressure difference between the bulk solution and the dimple, where the reverse curvature of the droplet sets up a Laplace pressure. This positive Laplace pressure drives film drainage to equilibrium, where a thin aqueous film of uniform thickness is stabilized by double-layer repulsion between the similarly charged oil droplet and the silica surface. The equilibrium film thickness is proportional to the range of the double-layer repulsion and decreases with more added $C_{12}E_8$ as a result of partitioning of surfactant at the oil−water interface.

Introduction

Film drainage at a deformable interface is an important phenomenon in emulsion systems such as food and paints and solvent extraction, and in other areas such as tertiary oil recovery. Rapid drainage and eventual film rupture are sometimes desired in applications such as solvent extraction, tertiary oil recovery, and liquid−membrane separations. In other areas such as food and paint, film instability is undesirable since it leads to a reduction in product shelf life and quality.

When two interfaces approach each other, for example, two droplets, in an emulsion system, a thin film forms. As film drainage proceeds, the film eventually reaches a thickness where surface forces such as van der Waals, double-layer, and steric forces become significant.[1] The system is stable or metastable when a film of uniform thickness is maintained over a long time period.[2,3] The thickness of the equilibrium film is dependent upon the magnitude of intersurface repulsive forces acting between the interfaces that bound the film. If, however, these forces are attractive, the film continues to thin until it reaches what is termed the critical film thickness, at which point an instability occurs and the film ruptures.[4]

Film drainage at a deformable droplet interface is dependent on the buoyancy of the droplet and droplet size and, more interestingly, is complicated by the complex interplay between hydrodynamics and interfacial forces.[5−9] Early work[10−17] and, more recently, work in our labs[6−9] has shown that when a spherical fluid droplet in a fluid continuous phase approaches an interface, the rate of film drainage is not everywhere uniform and is dependent on film thickness as defined by the curvature of the droplet. Typically, at the center of the droplet, which is the point of closest approach to the interface with which it interacts, film drainage is hindered relative to drainage at the droplet periphery, and the droplet becomes dimpled at that point.[6−9,18,19]

Recently, we have shown that imaging ellipsometry[20] can be used to profile deformable interfaces on approach of an oil droplet to a solid surface in a continuous aqueous

* To whom correspondence should be addressed.
† School of Chemistry.
‡ Department of Chemical Engineering.

(1) Ivanov, I. B. *Thin Liquid Films*; Marcel Dekker Inc.: New York, 1988.
(2) Binks, B. P. *Modern Aspects of Emulsion Science*; The Royal Society of Chemistry: Cambridge, U.K., 1998.
(3) Hiemez, P. C.; Rajagopalan, R. *Principles of Colloid and Surface Chemistry*, 3rd ed.; Marcel Dekker Inc.: New York, 1997.
(4) Blake, T. D.; Kitchener, J. A. *J. Chem. Soc., Faraday Trans.* **1972**, *68*, 1435−1442.
(5) Jeffreys, G. V.; Davies, G. A. In *Recent Advances in Liquid−Liquid Extraction*; Hanson, C., Ed.; Pergamon Press: Oxford, 1971; pp 495−583.
(6) Goodall, D. G.; Stevens, G. W.; Beaglehole, D.; Gee, M. L. *Langmuir* **1999**, *15*, 4579−4583.
(7) Goodall, D. G.; Stevens, G. W.; Beaglehole, D.; Gee, M. L. *Langmuir* **2002**, *18*, 4729−4735.
(8) Gee, M. L.; Goodall, D. G.; Stevens, G. W. *Oil Gas Sci. Technol.* **2001**, *56*, 33−40.
(9) Goodall, D. G.; Stevens, G. W.; Gee, M. L. *Langmuir* **2001**, *17*, 3784−3787.
(10) Hartland, S. *Trans. Inst. Chem. Eng.* **1967**, *45*, T102−T108.
(11) Burill, K. A.; Woods, D. R. *J. Colloid Interface Sci.* **1973**, *2*, 35−51.
(12) Hartland, S. *Chem. Eng. Sci.* **1967**, *22*, 1675−1687.
(13) Hartland, S. *J. Colloid Interface Sci.* **1968**, *26*, 383−394.
(14) Allan, R. S.; Mason, S. G. *Trans. Faraday Soc.* **1961**, *57*, 2027−2040.
(15) Platikanov, D. *J. Phys. Chem.* **1967**, *68*, 3619−3924.
(16) Hodgson, T. D.; Woods, D. R. *J. Colloid Interface Sci.* **1969**, *30*, 94−108.
(17) Hodgson, T. D.; Woods, D. R. *J. Colloid Interface Sci.* **1969**, *30*, 429−446.
(18) Fisher, L. R.; Hewitt, D.; Mitchell, E. E.; Ralston, J.; Wolfe, J. *Adv. Colloid Interface Sci.* **1992**, *39*, 397−416.
(19) Hewitt, D.; Fornasiero, D.; Ralston, J.; Fisher, L. R. *J. Chem. Soc., Faraday Trans.* **1993**, *89*, 817−822.
(20) Beaglehole, D. *J. Phys. Chem.* **1989**, *93*, 893−899.

10.1021/la0270237 CCC: $25.00
Published on Web 08/13/2003

phase.[6−9] Imaging ellipsometry/reflectometry has major advantages over other techniques such as interferometry in that it gives a more accurate measure of film thickness and is capable of measuring the film thickness profile across a droplet approaching an interface in real time until the point of film rupture.[6−9] In this earlier work, we used imaging ellipsometry/reflectometry to profile the shape of a deformable oil droplet approaching a silica surface in a continuous aqueous phase. We showed that, in such a system, an equilibrium film is formed with a thickness dependent on double-layer interactions between the solid surface and the droplet.[6−9] We also showed that, in this system, where the interfacial tension is constant and interfacial tension gradients across the interface are absent, the rate of film drainage is governed solely by hydrodynamics effects: At large film thicknesses, drainage is independent of electrolyte concentration. However, when the film thins, double-layer interactions become significant and influence the drainage rate via the effect of these forces on film thickness.[6,7]

In the present study, we have extended our earlier work to explore the effects of surfactants on film drainage in the same silica/water/oil system. Specifically, we investigate the drainage of an aqueous film containing nonionic surfactant on approach of a squalene droplet to a silica surface. Hence, we focus the study on how the addition of nonionic surfactant affects film stability and how variations in interfacial tension and the possibility of interfacial tension gradients and surface elasticity affect the dynamics of film drainage. To this end, we study film drainage as a function of surfactant concentration, the surfactant of choice being octaethylene glycol monodedecyl ether, i.e., $C_{12}E_8$.

Experimental Section

General Theory of Ellipsometry and Reflectometry. Ellipsometry is a well-known technique, the theory of which is well covered elsewhere.[21] We mention only some key points here. Briefly, in ellipsometry, one essentially measures two angles, Δ and Ψ, which express the change in polarization of a monochromatic light beam upon reflection from a film-covered surface.[21] In the system studied in the present work, the squalene droplet is the substrate and the thickness of an aqueous film between the droplet and a silica surface is probed. The ellipsometric angles Δ and Ψ are related to the ratio, ρ, of the complex amplitude Fresnel reflection coefficients, R_p and R_s, for p and s polarized light, respectively, viz.,[21]

$$\rho = R_p/R_s = \tan \psi e^{i\Delta} \quad (1)$$

In reflectometry, film thickness can be obtained from the measurement of the intensity of an unpolarized light beam reflected from a film-covered surface. The ratio of the intensity of the light reflected to the intensity of the incident light is known as reflectance, R_f, and, for a film covered surface, is related to the Fresnel reflection coefficients by

$$R_f = (1/2)(R_p^2 + R_s^2) \quad (2)$$

Imaging Ellipsometery and Experimental Procedure. Droplet/film profiling was performed using a modified imaging ellipsometer from Beaglehole Instruments Inc. The details of this imaging ellipsometer and experimental procedure have been described elsewhere.[6−8] Briefly, an oil droplet is rapidly formed at the tip of a stainless steel capillary of 0.8 mm inner diameter and placed at a set distance from a silica surface in an aqueous continuous phase. A droplet thus formed at the tip of the capillary has a controlled volume of 20 μL. In the present study, the droplet remains attached at the capillary for the duration of film drainage.

(21) Azzam, R. M. A.; Bashara, N. M. *Ellipsometry and Polarised Light*; North-Holland Inc.: New York, 1977.

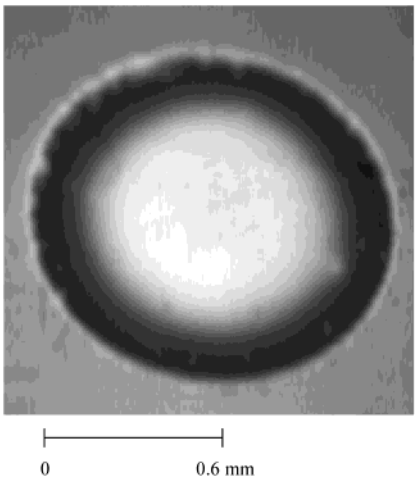

Figure 1. Typical gray-scale image of an oil droplet approaching a silica surface in an aqueous continuous phase containing nonionic surfactant. The graduation in gray scale is indicative of the variation in thickness of the film between the droplet and the solid surface. The darker the area, the thinner the film. Thus, in this case, the film is much thinner at the barrier ring of the droplet than at the center. This type of gray-scale image is typically obtained when the oil−water interface has deformed such that the droplet is dimpled at its center.

The ellipsometric measurements are taken after expansion of the drop as drainage of the aqueous film occurs on approach of the oil droplet to the silica surface. All experiments were carried out at room temperature of 21 °C.

We have described imaging ellipsometry in previous publications,[6−8] but will repeat this description here in brief for clarity. Imaging ellipsometry differs from conventional ellipsometry in that a beam area of approximately 1 cm^2 is employed, rather than the usual laser light source of area 1 mm^2. In addition, a condensing lens, objective lens, and CCD detector are inserted into the optical lineup. This combination allows simultaneous sampling of the entire droplet area, thereby facilitating accurate determination of the film profile over this entire area in real time.

By variation of the polarization of the incident light, two optical images are obtained: one polarized and one unpolarized. The polarized image gives the coefficient of ellipticity over the sample surface, whereas the unpolarized image is used when reflectometry is utilized, necessary when a film is very thick. This image is of reflected intensity, i.e., a gray-scale image. A typical gray-scale image is shown in Figure 1 for an aqueous film between an oil droplet and a solid surface. The variation of the reflected intensity and hence film thickness is revealed by the variation of the gray scale of the image, ranging from white, which corresponds to a very thick film, to black, which corresponds to a very thin Newton black film. Note that the image presented in Figure 1 clearly shows that the drop is dimpled at its center. In the analysis of the gray-scale images, a film profile is obtained by taking a cross-section through the image and calculating the film thickness along the cross-section. When calculating film thickness, we correct for the presence of surfactant in the film by using the measured refractive indices of 1.333, 1.334, and 1.341, corresponding to surfactant concentrations of 3.5×10^{-6}, 1.0×10^{-5}, and 6.5×10^{-5} M, respectively, as done previously.[8]

Materials and Cleaning Methods. Squalene ($C_{30}H_{50}$) was obtained from Sigma Aldrich Chemical Co. Pty, Ltd. (> 98%) and was furthered purified via vacuum distillation. Octaethylene glycol monododecyl ether ($C_{28}H_{58}O_9$), commonly known as $C_{12}E_8$, was obtained from Sigma Aldrich with a purity of ≥98% and was used as received. All surfactant solutions were made up in Milli-Q water with a conductivity of 18 MΩ cm and a pH of 5.6, i.e., natural pH. No electrolyte was added.

The silica surface was suprasil grade (refractive index 1.458) and was supplied by Ealing Optics. It was removed of impurities by flushing with a warm solution of Extran 100 and then rinsed with Milli-Q water. This was followed by treatment with a hot

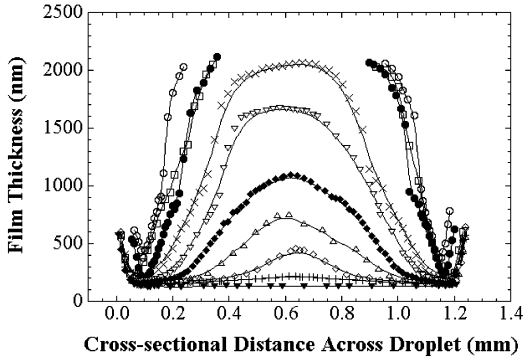

Figure 2. Cross-sections taken through a gray-scale image, such as that in Figure 1, yield a profile of the film. This figure contains a series of such profiles taken at various times during the drainage of an aqueous film containing 3.5×10^{-6} M $C_{12}E_8$ confined between a squalene droplet and a silica surface which the droplet is approaching at pH 5.6. Typically a continuum of profiles are obtained, but only a few are shown for clarity, taken at 0.003 h (○), 0.028 h (●), 2.137 h (□), 4.304 h (×), 5.346 h (▽), 6.096 h (◆), 7.096 h (△), 8.235 h (◇), 8.735 h (+), and 21.985 h (▼).

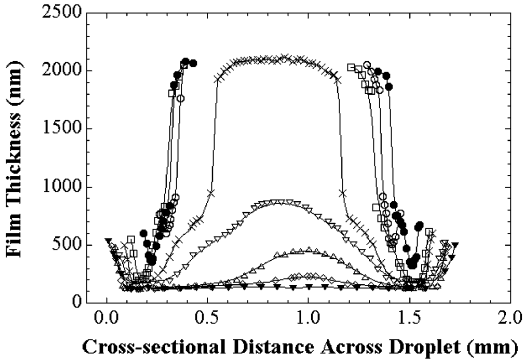

Figure 3. A series of film profiles obtained from the gray-scale images, as done for Figure 2, at various times during the drainage of an aqueous film containing 1.0×10^{-5} M $C_{12}E_8$ confined between a squalene droplet on approach and a silica surface which the droplet is appraoching at pH 5.6. Typically a continuum of profiles are obtained, but only a few are shown for clarity, taken at 0.004 h (○), 0.271 h (●), 2.671 h (□), 5.188 h (×), 7.521 h (▽), 13.354 h (△), 16.521 h (◇), and 23.521 h (▼).

ammoniacal peroxide solution for about 1 h followed by copious rinsing with Milli-Q water.

The stainless steel capillary was soaked in an Extran solution for 12−24 h and then rinsed with Milli-Q water followed by immersion in a nitric acid bath and then copious rinsing with Milli-Q water. All other fittings and glassware, including the syringe and glass cell, were washed in Extran solution for 12 h before copious rinsing with Milli-Q water. They were then soaked in concentrated sodium hydroxide solution for 2 h and then rinsed again with Milli-Q water.

Results and Discussion

Film Profiles. The effects of nonionic surfactant on the drainage of an aqueous film between a squalene droplet and a hydrophilic, negatively charged silica surface which the droplet is approaching were investigated. Film drainage was monitored at three surfactant ($C_{12}E_8$) concentrations in the aqueous phase, i.e., 3.5×10^{-6}, 1.0×10^{-5}, and 6.5×10^{-5} M. Previously, the cmc of this surfactant has been found to be 1.0×10^{-4} M.[22−24] The corresponding film thickness profiles obtained are shown in Figures 2−4, respectively. Note that, during the experiment, a continuum of film profiles is obtained. Only a few are plotted in these figures for the sake of clarity.

The profile plots of Figures 2−4 clearly show that, on initial approach of the droplet to the surface, the droplet immediately deforms into a dimpled shape. Note, that during the initial stages of film drainage, at film thicknesses >2000 nm, the high degree of droplet curvature somewhat erodes the optical clarity of the gray-scale image. Hence, drainage profiles cannot be resolved across these high-curvature regions and are discontinuous.

The formation of a dimple during film drainage at a deformable interface has been observed previously.[6−8,11,18,19] The evolution of the droplet shape as film drainage occurs depends on the deformability of both the droplet and the interface to which it approaches. The extent of deformation is, in turn, dependent on the viscosity of the continuous phase, interfacial tension, surface elasticity, droplet radius, and density difference between the droplet and the continuous phase. Earlier work[6−8,11,18,19] has shown

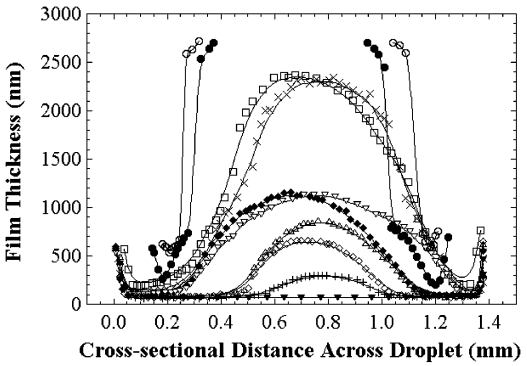

Figure 4. A series of film profiles obtained from the gray-scale images, as done for Figure 2, at various times during the drainage of an aqueous film containing 6.5×10^{-5} M $C_{12}E_8$ between a squalene droplet and a hydrophilic silica surface which the droplet is approaching at pH 5.6. Typically a continuum of profiles are obtained, but only a few are shown for clarity, taken at 0.007 (○), 0.294 h (●), 4.044 h (□), 6.233 h (×), 9.403 h (▽), 12.922 h (◆), 24.284 h (△), 25.933 h (◇), 31.908 h (+), and 45.658 h (▼).

that when an initially spherical droplet approaches a surface, the rate at which film drainage occurs is not everywhere uniform. At the periphery of the droplet, i.e., the barrier ring, the film is thick, whereas the center of the film is relatively thin since this is the point of closest approach of the droplet to the surface. Consequently, drainage from the barrier ring is opposed by a relatively small viscous drag compared to drainage at the film's center. This nonuniform film drainage results in excess liquid at the center of the film, which deforms the film−droplet interface; i.e., the droplet dimples.

An interesting observation when the drainage profiles (Figures 2−4) are compared is that the degree of spreading at the barrier ring, i.e., the increase in the film area, depends on the $C_{12}E_8$ concentration. At 3.5×10^{-6} M $C_{12}E_8$ (Figure 2), the degree of spreading is approximately uniform over the barrier ring throughout the entire drainage process. The dimple evolves uniformly, remaining at the center of the film. At the intermediate $C_{12}E_8$ concentration of 1.0×10^{-5} M (Figure 3), some nonuniformity in spreading at the barrier ring occurs, as evidenced by the different film areas at either side of the profile, and is most noticeable during the latter stages of film drainage. This is also the case at 6.5×10^{-5} M $C_{12}E_8$ (Figure 4), where there is a large degree of spreading at

(22) Lu, J. R.; Li, Z. X.; Thomas, R. K.; staples, E. J., Thompson, L.; Tucker, I.; Penfold, J. *J. Phys. Chem.* **1994**, *98*, 6559−6567.
(23) Lin, S. Y.; Tsay, R. Y.; Lin, L. W.; Chen, S. I. *Langmuir* **1996**, *12*, 6530−6536.
(24) Tan, C. S. Thesis, University of Melbourne, Melbourne, Australia, 2001.

the barrier ring, so the region over which the film is dimpled is small.

Nonuniform film drainage, which involves nonuniform spreading at the barrier ring, is most marked at 6.5×10^{-5} M $C_{12}E_8$ (Figure 4), where, clearly, spreading is much greater to the left of the profile. Note also that the position of the dimple moves with time across the film profile from left to right: spreading and the consequential increase in film area that occurs, predominately to the left of the profile, cause the trapped fluid at the dimple to flow in a direction where there is a lower opposing force to fluid flow, i.e., where the degree of spreading at the barrier ring is small. Therefore, we observe the position of the dimple to change, moving from the left of the profile where spreading is greatest, toward the right of the profile where spreading is least. The effects of spreading on the rate of film drainage are discussed in detail below under Film Drainage.

The increase in nonuniform spreading with increasing surfactant concentration is largely due to the lowering of the interfacial tension between the squalene drop and the aqueous continuous phase. The lower the interfacial tension, the less energy required to deform the interface.[25] Hence, the degree of droplet deformation increases as interfacial tension decreases.

Stabilization of the Equilibrium Film. At each surfactant concentration studied, film drainage occurs until, eventually, the dimpled film evolves into a stable equilibrium thin film of uniform thickness. Film stability is the result of a net repulsive force between the oil−aqueous and silica−aqueous interfaces, which opposes any further thinning of the film. This repulsive force is attributed to a dominant double-layer interaction between the droplet and the silica surface interacting across the aqueous surfactant solution.[6,7] We arrive at this conclusion on the basis of earlier studies[26,27] which have shown that organic droplets dispersed in an aqueous phase bear a net negative surface charge, as does silica. The origin of this charge is not the focus of this paper, but we should mention that it is thought to arise from adsorption of hydroxyl ions at the oil−aqueous or air−aqueous interface. We therefore expect the squalene−aqueous interface to have a negative surface potential in the range of −20 to −50 mV, on the basis of electrokinetic measurements of oil droplets in aqueous solution as a function of pH.[28] At pH 5.6, the pH of the aqueous phase used in the present study, silica also has a negative surface potential of approximately −40 mV.[29]

However, we have found, that in our system of an oil droplet interacting with a silica surface across a nonionic surfactant solution, the film thickness at equilibrium is a function of surfactant concentration. Indeed, the equilibrium film thickness decreases with increasing surfactant concentration, implying a reduction in the range and magnitude of double-layer repulsion between silica and the oil−water interface. Refer to the data in Table 1.

Direct force measurements[30,31] have shown that adsorption of nonionic surfactant at a silica or mica surface has little or no effect on the surface potential. Interaction forces measured[30] between two silica surfaces in water with 0.1% added $C_{12}E_5$ show that the surface interaction is dominated by a double-layer repulsive force at surface separations above 15 nm and this double-layer interaction has a range and decay comparable to what is observed in the absence of surfactant. Similar results were obtained for the interaction between two mica surfaces in an aqueous solution of $C_{12}E_4$ at a concentration nearly twice its cmc.[31] It is therefore safe to assume that, in our study, the adsorption of $C_{12}E_8$ will not alter the surface potential of silica. However, an increase in the surfactant surface excess at the squalene−aqueous interface reduces the surface area available for anion adsorption, which is the source of charge at this interface, as mentioned above. Thus, the charge at this interface is lowered and so too its surface potential. It is the decrease in charge at the squalene−aqueous interface that is primarily responsible for the reduction in double-layer repulsion between the squalene drop and the silica surface as surfactant concentration is increased and hence the variation in equilibrium film thickness with surfactant concentration. This conclusion is consistent with electrokinetics measurements[32,33] which show that the surface potential at the oil−aqueous interface decreases in magnitude as nonionic surfactant concentration increases. To illustrate this consistency, we have taken values of potential at the oil−water interface from these studies at surfactant concentrations comparable to those used in our work and listed these in Table 1.

Table 1. Equilibrium Thickness of an Aqueous Film Given as a Function of the Concentration of $C_{12}E_8$[a]

concn of $C_{12}E_8$ (M)	exptl equilibrium film thickness (nm)	surface potential at the oil−aqueous interface[32] (mV)
3.5×10^{-6}	134	−45
1.0×10^{-5}	122	−40
6.5×10^{-5}	71	−20

[a] The film is stabilized between a squalene droplet and a silica surface by double-layer repulsion. The surface potential at an oil−water interface has been measured previously as a function of the concentration of the nonionic surfactant $C_{12}E_4$.[32] Data from ref 32 have been quoted in this table to highlight the effects of surface potential at the oil−water interface on the equilibrium film thickness. It is this potential that brings about variation in the equilibrium film thickness since the surface potential of silica is little affected by the addition of $C_{12}E_8$.

Film Drainage. In the analysis of the drainage rate at the barrier ring, we take an average of the minimum film thickness on both the left- and right-hand sides of the profile as a function of time, rather than the film thickness at a fixed point along the profile. This method of rate analysis is adopted to avoid vagaries that would otherwise be introduced to the analysis as a result of nonuniform spreading that causes the dimple to essentially sweep across the profile with time, as described above and seen in the profile plots (Figures 2−4). Drainage rate data thus obtained are shown in Figure 5, plotted on a semilog scale. Drainage at the barrier ring at each $C_{12}E_8$ concentration, i.e., 3.5×10^{-6}, 1.0×10^{-5}, and 6.5×10^{-5} M, consists of five different stages, all of first-order kinetics, where consecutive stages are distinguished by a transition from one drainage rate to another. The corresponding gradients of each stage are representative of the drainage rate. These are summarized in Table 2.

(25) Hunter, R. J. *Foundations of Colloids Science*; Oxford University Press: Oxford, U.K., 2001.
(26) Carruthers, J. C. *J. Chem. Soc., Faraday Trans.* **1938**, *34*, 300−307.
(27) Dickinson, W. *J. Chem. Soc., Faraday Trans.* **1941**, *37*, 140−148.
(28) Gu, Y.; Li, D. Q. *J. Colloid Interface Sci.* **1998**, *206*, 346−349.
(29) Somasundaran, P.; Snell, E. D.; Fu, E.; Xu, Q. *Colloids Surf.* **1992**, *63*, 49−54.
(30) Tiberg, F.; Ederth, T. *J. Phys. Chem. B* **2000**, *104*, 9689−9695.
(31) Giasson, S.; Kuhl, T. L.; Israelachvili, J. N. *Langmuir* **1998**, *14*, 891−898.
(32) Marinova, K. G.; Alargova, R. G.; Denkov, N. D.; Velev, O. D.; Petsev, D. N.; Ivanov, I. B.; Borwankar, R. P. *Langmuir* **1996**, *12*, 2045−2051.
(33) Manev, E.; Pugh, R. J. *Langmuir* **1991**, *7*, 2252−2260.

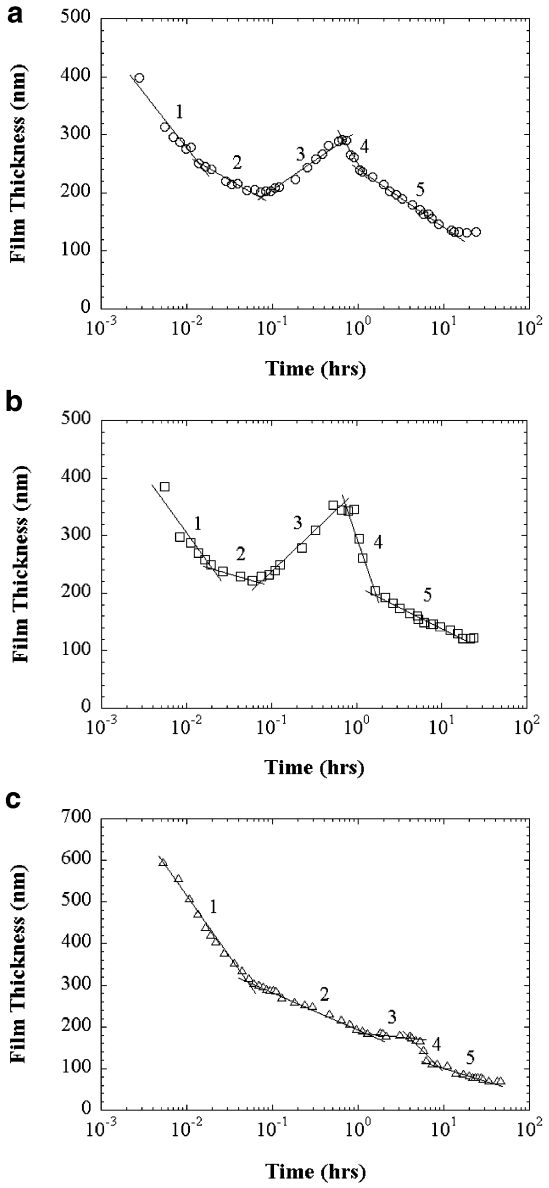

Figure 5. Film thickness at the barrier ring plotted as a function of time, on a semilog scale, for $C_{12}E_8$ concentrations of (a, top) 3.5×10^{-6} M (○), (b, middle) 1.0×10^{-5} M (□), and (c, bottom) 6.5×10^{-5} M (△). Note that film drainage at the barrier ring occurs as a sequence of stages, each distinguished by the drainage rate, which is proportional to the gradient of the plot. The solid lines are the gradients drawn as a guide to the eye. The numbering of the gradients corresponds to the drainage rates at each stage listed in Table 2.

Table 2. Drainage Rate Constants during Each Stage of Film Drainage at the Barrier Ring at Each Surfactant Concentration[a]

	gradient/drainage rate at the barrier ring		
stage	3.5×10^{-6} M $C_{12}E_8$	1.0×10^{-5} M $C_{12}E_8$	6.5×10^{-5} M $C_{12}E_8$
1	−77.82	−99.65	−126.20
2	−24.77	−20.47	−38.58
3	47.29	54.55	−9.55
4	−110.03	−189.96	−108.39
5	−42.82	−32.86	−29.40

[a] Note that the error in the data is estimated to be 10%. These data are obtained from the gradients of the semilog plots of film thickness at the barrier ring versus time in Figure 5.

For stage 1, the average drainage rates at each $C_{12}E_8$ concentration are similar within the estimated error of 10%. During this stage, the corresponding measured film thickness ranges from about 300 to 600 nm. Double-layer repulsion will be very weak or negligible over this range of film thicknesses, as previously shown.[30,31,34] Hence, interfacial tension and hydrodynamic factors such as viscosity and droplet buoyancy will determine the rate of film drainage.[35] We have measured the bulk viscosity of the aqueous phase and droplet buoyancy to be independent of surfactant concentration. The interfacial tension at the oil−water interface is the only property differentiating each system, yet clearly, during stage 1, the similarity in the drainage rates indicates that this has little or no effect on film drainage at this stage.

The transition from stage 1 to stage 2 is marked by a decrease in the drainage rate (see Table 2) at a film thickness we call the "transition thickness". The rates are similar at the lower surfactant concentrations (3.5×10^{-6} and 1.0×10^{-5} M), but the rate is an order of magnitude lower at the high $C_{12}E_8$ concentration (6.5×10^{-5} M). The surfactant concentration dependence of the drainage rate indicates that hydrodynamic factors that control the initial drainage rate no longer dominate. We attribute this transition in drainage rate to the onset of double-layer repulsion between the silica surface and oil droplet, which acts to oppose drainage. The transition from stage 1 drainage to stage 2 occurs at film thicknesses of 255, 260, and 300 nm for surfactant concentrations of 3.5×10^{-6}, 1.0×10^{-5}, and 6.5×10^{-5} M, respectively, well within the range of a double-layer interaction. Double-layer forces in this type of system are weak over this range and are difficult to detect via conventional mechanical direct force measuring techniques such as the use of the surface forces apparatus (SFA) and atomic force microscope (AFM).[30,31] However, we have discussed in an earlier publication[7] that, in our experiment, the oil−water interface essentially acts as an infinitely weak spring, the stiffness of which is dependent on the interfacial tension. Hence, surface forces are detectable over a longer range than possible with the SFA or AFM.

At the two lower surfactant concentrations, i.e., 3.5×10^{-6} and 1.0×10^{-5} M $C_{12}E_8$, the drainage rates (see Table 2) and transition thicknesses (255 nm and 260 nm, respectively) are the same within experimental error. This is consistent with our model of the effect of double-layer repulsion on film drainage.[6,7] Double-layer repulsion is essentially the same at each of these $C_{12}E_8$ concentrations since the electrostatic potentials at the silica−aqueous interface[29] are identical, i.e., −45 mV, at both these surfactant concentrations and the potential at the oil−aqueous interface is −45 mV at 3.5×10^{-6} M and marginally smaller, i.e., −40 mV, at 1.0×10^{-5} M $C_{12}E_8$.[32] Hence, the film thicknesses at which double-layer forces first affect film drainage, i.e., the transition from stage 1 to stage 2, are comparable.

Interestingly, the effect of double-layer repulsion alone is insufficient to explain the transition thickness of 300 nm at 6.5×10^{-5} M $C_{12}E_8$, where the potentials at the silica−aqueous and oil−aqueous interfaces are −35 and −20 mV, respectively.[29,32] One would expect, on the basis of these potentials, a significant reduction in the range of double-layer repulsion, which should therefore result in a thinner film at the transition point compared to the lower surfactant concentrations. However, the transition point occurs at a higher film thickness (300 nm) than observed at the lower surfactant concentrations, as shown in Figure 5.

(34) Rutland, M. W.; Senden, T. J. *Langmuir* **1993**, *9*, 412−418.
(35) Ivanov, I. B. *Pure Appl. Chem.* **1980**, *52*, 1241−1262.

Hence, at high $C_{12}E_8$ concentrations additional factors must contribute to the point of transition from stage 1 to stage 2. It is known that adsorbed nonionic surfactants form surface aggregates at bulk concentrations below, but close to, the cmc.[34,36] According to Tiberg,[36] $C_{12}E_8$ forms surface aggregates at the silica−aqueous interface at a bulk concentration of 6.0×10^{-5} M. It is also thought that aggregates form at the oil−aqueous interface.[36] Therefore, in the present study, aggregates are present when the surfactant concentration is 6.5×10^{-5} M but absent at the lower surfactant concentrations of 3.5×10^{-6} and 1.0×10^{-5} M.[34,36] It is postulated that, at 6.5×10^{-5} M $C_{12}E_8$, aggregates at each interface and in the film volume impose some resistance to the fluid flow from the barrier ring, possibly by increasing viscosity within the film and at the interface, thus lowering the drainage rate. These viscous effects are absent at the lower surfactant concentrations since aggregation does not occur.

Table 2 shows that during the latter stages of film drainage (stages 3−5), the drainage at 6.5×10^{-5} M $C_{12}E_8$ is approximately an order of magnitude slower than at the lower surfactant concentrations. Surfactant aggregation, mentioned above, will certainly play a part in this result, but there are other factors that also contribute during these stages. Another issue that becomes significant during the latter stages of drainage is the relative thickness of the film at the barrier ring. At 6.5×10^{-5} M $C_{12}E_8$, the film thickness is only around half that at the other surfactant concentrations. Thus, the smaller film volume also increases viscous drag and so hinders fluid flow. Additionally, and possibly more importantly, spreading at the barrier ring will hinder fluid flow. The degree of spreading at each surfactant concentration is contrasted very clearly the profile plots, Figures 2−4, are compared and becomes increasingly more pronounced as surfactant concentration increases.

When spreading at the barrier ring is significant, as is the case at 6.5×10^{-5} M $C_{12}E_8$, one would expect hindered fluid flow, since flow through the spreading barrier ring is essentially equivalent to flow through two parallel plates. Although the velocity of flow is unknown in this case, we can assume that flow between the droplet and the silica surface is laminar. This is a reasonable assumption since the Reynolds number, $(\rho d/\mu)u$, for our system is $0.103u$. ρ, d, and μ are the density, width, and viscosity of the film, respectively. u is the velocity of flow. Clearly, any accessible velocity for our experiment will result in laminar flow characteristics. Thus, for laminar flow between two parallel plates, the Navier−Stokes equation yields[37]

$$Q = \frac{2(h/2)^3}{3\mu}\left(\frac{\Delta P}{x}\right) \tag{3}$$

where Q is the flow rate between parallel plates and μ is the viscosity of the fluid which flows through a gap of width x and thickness $h/2$. x and h are equivalent to the width and thickness of the barrier ring, respectively. ΔP is the difference in hydrostatic pressure between the center of the film where it is dimpled and outside the barrier ring over the flow distance of x, i.e, the width of the barrier ring. Equation 3 assumes that μ and ΔP remain constant during spreading, so Q is affected only by changes in spreading at the barrier ring, i.e., a change in x, or h. Clearly, under these conditions, the greater the degree of spreading, the slower the flow rate, so film drainage is hindered. Note that ΔP used in eq 3 is the Laplace pressure that results from the reverse curvature of the oil−water interface and, as implied above, is a positive pressure that acts to drive the fluid out from the dimple.[3,6,7] For a spherically symmetric interface of radius of curvature R_c, the Young−Laplace equation states that[25]

$$\Delta P = 2\gamma/R_c \tag{4}$$

where γ is the interfacial tension. In the present study, the interfacial tension at the oil−water interface for 3.5×10^{-6}, 1.0×10^{-5}, and 6.5×10^{-5} M $C_{12}E_8$ was measured to be 16.5×10^{-3}, 13.5×10^{-3}, and 4.3×10^{-3} N/m, respectively.

In light of the considerations of flow through the barrier ring, above, we now draw attention to the rate of drainage from the center of the drop, presented in Figure 6. This figure shows that, at the center, film drainage consists of a sequence of consecutive stages distinguished by a transition from one drainage rate to another, as also seen for drainage at the barrier ring detailed above. Note that the number of stages depends on surfactant concentration, so the labeling of each stage takes this into account for ease of comparison. As before, drainage rates are obtained from the gradient of the plots in Figure 6 at each stage and are summarized in Table 3.

From one stage to another, the variation in the rate of fluid flow from the drop's center can be explained by considering the Laplace pressure (eq 4) and the effect of spreading at the barrier ring (eq 3). In the calculation of ΔP, radii of curvature were obtained directly from the droplet profiles, i.e., Figures 2−4, under the assumption

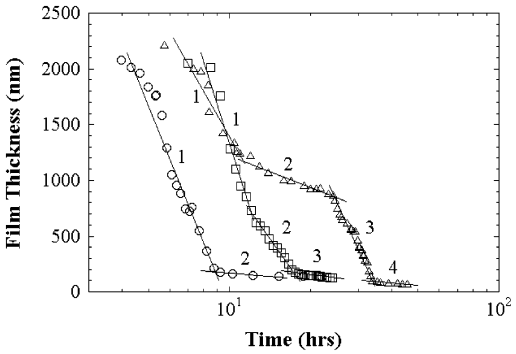

Figure 6. Film thickness at the droplet's center plotted as a function of time, on a semilog scale, for $C_{12}E_8$ concentrations of 3.5×10^{-6} M (○), 1.0×10^{-5} M (□), and 6.5×10^{-5} M (△). Note that film drainage at the center of the droplet occurs as a sequence of stages, each distinguished by the drainage rate, which is proportional to the gradient of the plot. The solid lines are the gradients drawn as a guide to the eye. The numbering of the gradients corresponds to the drainage rates at each stage listed in Table 3.

Table 3. Drainage Rate Constants during Each Stage of Film Drainage at the Drop's Center at Each Surfactant Concentration[a]

	gradient/drainage rate at the drop's center		
stage	3.5×10^{-6} M $C_{12}E_8$	1.0×10^{-5} M $C_{12}E_8$	6.5×10^{-5} M $C_{12}E_8$
1	−2629.36	−2854.85	−1540.01
2	−38.11	−84.529	−337.85
3		−5.405	−2050.73
4			−93.38

[a] Note that the error in the data is estimated to be 10%. These data are obtained from the gradients of the semilog plots of film thickness at the drop's center versus time in Figure 6.

(36) Tiberg, F. *J. Chem. Soc, Faraday Trans.* **1996**, *92*, 531−538.
(37) Wilkes, J. O. *Fluid Mechanics for Chemical Engineers*; Prentice Hall: Upper Saddle River, NJ, 1999.

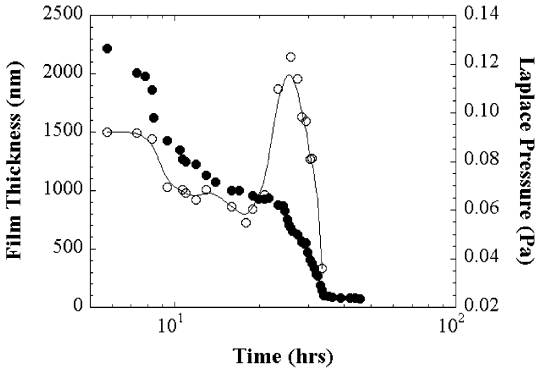

Figure 7. Film thickness at the drop's center (●) and the Laplace pressure within the dimple (○) as a function of time, at 6.5×10^{-5} M $C_{12}E_8$. Note that significant changes in Laplace pressure correspond to transitions in the drainage rate from one stage to another, such that the drainage rate is directly proportional to the Laplace pressure.

of spherical symmetry to yield the Laplace pressure, ΔP, as a function of film thickness at each surfactant concentration. ΔP values are similar at both 3.5×10^{-6} and 1.0×10^{-5} M $C_{12}E_8$ and increase linearly with time. This accounts for the relatively simple drainage behavior at the center shown in Figure 6 and the similarity in the drainage rate during stage 1(see Table 3) at these two surfactant concentrations. Therefore, transitions in drainage rate must be due to spreading at the barrier ring, which opposes the Laplace pressure. At 3.5×10^{-6} M $C_{12}E_8$, drainage has only one transition in rate. This is the transition from stage 1 to the final stage, stage 2, which occurs once the barrier ring is at its equilibrium thickness. At 1.0×10^{-5} M $C_{12}E_8$, there are only two transitions in rate: the transition from stage 1 to stage 2 marks the onset of significant spreading at the barrier ring. The transition from stage 2 to the final stage, stage 3 in this case, occurs once the barrier ring is at its equilibrium thickness.

In contrast, Figure 6 and the data in Table 3 highlight the complicated transitions in drainage rate at the film's center when the surfactant concentration is high, i.e., at 6.5×10^{-5} M $C_{12}E_8$. Spreading at the barrier ring is a significant factor influencing the rate of drainage over all stages of drainage, as discussed above, and opposes Laplace pressure-driven flow. However, another factor is that, at this high surfactant concentration, the oil−aqueous interface has a lower interfacial tension, which affects interfacial deformation. This increases the degree of spreading but also affects the Laplace pressure, making it a complex function of time, in contrast to what is obtained at the lower surfactant concentrations discussed in the above paragraph. To illustrate this, Figure 7 contains a plot of both film thickness and Laplace pressure versus time at 6.5×10^{-5} M $C_{12}E_8$. Note that the first significant decrease in Laplace pressure, at around 10 h, corresponds to the point of transition from stage 1 to stage 2 and a reduction in the drainage rate. The marked increase in Laplace pressure at approximately 25 h corresponds to an increase in drainage rate and the transition from stage 2 to stage 3. The Laplace pressure tends to zero at 33 h, i.e., the transition from stage 3 to stage 4, since equilibrium is almost attained and the film has negligible curvature, i.e., $R_c \rightarrow \infty$.

Film Recovery. An interesting observation is that film recovery occurs during stage 3 at 3.5×10^{-6} and 1.0×10^{-5} M $C_{12}E_8$, indicated in Figure 5a,b by the increase in film thickness and by the positive gradients in Table 2; i.e., there is a reversal of fluid flow back into the barrier ring. This is not observed at 6.5×10^{-5} M $C_{12}E_8$. This result is reproducible over several repeat experiments. The droplet profiles at 3.5×10^{-6} and 1.0×10^{-5} M $C_{12}E_8$ (Figures 2 and 3) show that, during the reversal of film drainage, the size and shape of the dimple do not change. The implication is, therefore, that, to achieve reversed film recovery, fluid flows back into the barrier ring from the exterior of the film, which therefore increases the total volume of the film, thereby increasing the total time required to reach equilibrium.

Film recovery can be attributed to the Marangoni effect, in which interfacial tension gradients induce stresses in the system to restore or hinder film drainage by redistributing adsorbed surfactant molecules.[38−43] Since fluid flows through the barrier ring during film drainage, more surfactant is expected to accumulate at the periphery of the droplet, thus reducing the interfacial tension in this region and facilitating deformation at this part of the squalene−aqueous interface. Additionally, since the film is thinnest at the barrier ring, free surfactant becomes relatively concentrated. The resulting interfacial tension and bulk chemical potential gradients lead to a flow of fluid back into the barrier ring in an attempt to reattain a uniform chemical potential across the interface and within the film, thus increasing film thickness across this region.[38,43]

Film recovery has not been widely observed by others in film drainage studies; however, Shen and Hartland[38] have attempted to model this effect, basing their model on interfacial tension gradients. They found that reversal of film drainage is possible if the initial amount of surfactant occupies less than 30% of the interfacial area. Yeo et al.[43] have also modeled the dynamics of Marangoni-driven local film drainage between two drops and reported exactly the same result. These theoretical studies are consistent with the present work, where reversal of film drainage is only observed when the bulk concentration of surfactant is low. Film recovery is not observed at the high surfactant concentration, i.e., 6.5×10^{-5} M. See Figure 5c. Interfacial tension measurements made by us[23] show that, at this surfactant concentration, the oil−water interface is 89% saturated with surfactant. At high surfactant concentrations, shear-induced transfer of surfactant to the barrier ring and within the film can be rapidly offset by the diffusion of surfactant molecules back into regions that are transiently depleted of surfactant, thereby minimizing concentration gradients and so Marangoni flow.

After film recovery, drainage recommences, i.e., stage 4 in Figure 5a,b. Interestingly, however, the drainage rate at 1.0×10^{-5} M $C_{12}E_8$ is higher than that at 3.5×10^{-6} M $C_{12}E_8$ (Table 2). This result is sensible since, during stage 3, there is a greater degree of film recovery at the higher surfactant concentration. The film thickness peaks at around 390 nm, whereas at 3.5×10^{-6} M $C_{12}E_8$ the maximum is around 300 nm. Fluid flow is less hindered the thicker the film and hence the faster the rate of drainage at 1.0×10^{-5} M $C_{12}E_8$.

(38) Shen, H. H.; Hartland, S. *J. Colloid Interface Sci.* **1994**, *167*, 94−103.
(39) Velv, O. D.; Gurkov, T. D.; Borwankar, R. P. *J. Colloid Interface Sci.* **1993**, *159*, 497−501.
(40) Danov, K. D.; Gurkov, T. D.; Dimitrova, T.; Ivanov, I. B.; Smith, D. *J. Colloid Interface Sci.* **1997**, *188*, 313−324.
(41) Nierstrasz, V. A.; Frens, G. *J. Colloid Interface Sci.* **1998**, *207*, 209−217.
(42) Chesters, A. K.; Bazhlekov, I. B. *J. Colloid Interface Sci.* **2000**, *230*, 229−243.
(43) Yeo, L. Y.; Matar, O. K., Perez de Ortiz, E. S.; Hewitt, G. F. *J. Colloid Interface Sci.* **2001**, *241*, 233−247.

Conclusions

In this paper we present profiles in real time of a draining aqueous film confined between a squalene droplet and a solid silica surface. The profiles show that the droplet becomes dimpled at the center due to hydrodynamic forces, as seen before. Added nonionic surfactant ($C_{12}E_8$) does not affect dimple formation but affects the mode of film drainage. Lowering of the oil−water interfacial tension by the addition of $C_{12}E_8$ promotes nonuniform spreading at the barrier ring and hence nonuniform film drainage; i.e., the dimple "sweeps" across the film profile. During the course of drainage, the film evolves from a dimpled shape to a film of uniform thickness stabilized by double-layer repulsion. The equilibrium film thickness is proportional to the range of the double-layer repulsion and decreases with more added $C_{12}E_8$ as a result of partitioning of surfactant at the oil−water interface.

At low surfactant concentrations (<10% of the cmc), the Marangoni effect reverses the direction of fluid flow and we observe film recovery. At high surfactant concentrations, shear-induced transfer of surfactant to the barrier ring and within the film can be rapidly offset by the diffusion of surfactant molecules back into regions that are transiently depleted of surfactant, thereby minimizing concentration gradients and so Marangoni flow.

The rate of film drainage through the barrier ring and from the dimple can be explained in terms of the Hagen−Poiseuille law and, as such, is dependent on the extent to which spreading occurs and the hydrostatic pressure difference between the bulk solution and the dimple, since the reverse curvature of the droplet sets up a Laplace pressure. Drainage is driven by the positive Laplace pressure and is hindered by spreading at the barrier ring. At high surfactant concentrations where the interfacial tension is lowered and the oil−water interface is more deformable, the rate of drainage from the dimple is complex since the large degree of spreading decreases the radius of curvature of the dimple, increasing the Laplace pressure.

LA0270237